Available online at www.sciencedirect.com

ScienceDirect

Advances in Space Research 55 (2015) 125–134

ADVANCES IN SPACE RESEARCH (a COSPAR publication)

www.elsevier.com/locate/asr

A simplified and unified model of multi-GNSS precise point positioning

Junping Chen [a,*], Yize Zhang [a,b], Jungang Wang [a,b], Sainan Yang [a], Danan Dong [c], Jiexian Wang [b], Weijing Qu [a], Bin Wu [a]

[a] Shanghai Astronomical Observatory, Chinese Academy of Sciences, Shanghai 200030, PR China
[b] College of Surveying and Geo-informatics Engineering, Tongji University, Shanghai 200092, PR China
[c] School of Information Science & Technology, East China Normal University, Shanghai 200242, PR China

Received 6 July 2014; received in revised form 19 September 2014; accepted 7 October 2014
Available online 20 October 2014

Abstract

Additional observations from other GNSS s can augment GPS precise point positioning (PPP) for improved positioning accuracy, reliability and availability. Traditional multi-GNSS PPP model requires the estimation of inter-system bias (ISB) parameter. Based on the scaled sensitivity matrix (SSM) method, a quantitative approach for assessing parameter assimilation, we theoretically prove that the ISB parameter is not correlated with coordinate parameters and it can be assimilated into clock and ambiguity parameters. Thus, removing ISB from multi-GNSS PPP model does not affect coordinate estimation. Based on this analysis, we develop a simplified and unified model for multi-GNSS PPP, where ISB parameter does not need to be estimated and observations from different GNSS systems are treated in a unified way. To verify the new model, we implement the algorithm to the self-developed software to process 1 year GPS/GLONASS data of 53 IGS (International GNSS Service) worldwide stations and 1 month GPS/BDS data of 15 IGS MGEX (Multi-GNSS Experiment) stations. Two types of GPS/GLONASS and GPS/BDS combined PPP solution are performed, one is based on traditional model and the other implements the new model. RMSs of coordinate differences between the two type of solutions are few μm for daily static PPP and less than 0.02 mm for GPS/GLONASS kinematic PPP in the North, East and Up components, respectively. Considering the millimeter-level precision of current GNSS PPP solutions, these statistics demonstrate equivalent performance of the two solution types.

Keywords: Multi-GNSS; MGEX; Precise point position; Inter-system bias; Scaled sensitivity matrix

1. Introduction

Precise point positioning (PPP) using global positioning system (GPS) measurements achieves accuracy for static and kinematic stations at the millimeter to decimeter levels, respectively (Zumberge et al., 1997; Bisnath and Gao, 2009). With the development of navigation systems and tracking infrastructure, PPP using multi-system observations has become increasingly popular (Dach et al., 2009, 2010; Píriz et al., 2009; Melgard et al., 2009; Cai and Gao, 2013; Chen et al., 2013). Multi-GNSS (Global Navigation Satellite Systems) PPP could improve solution availability by improving tracking geometry, especially in environment like urban canyon and ravines. On the other hand, it improves positioning accuracy as it has more observations and it largely eliminate existing position errors introduced by the periodic regression of satellite constellations (Flohrer, 2008).

Many manufacturers are providing multi-GNSS receivers, however, most geodetic receivers and antennas are not calibrated, which leaves instrument hardware delay unknown. In the GPS-only data processing, the instrument hardware delay is assimilated into receiver clock and does not affect position estimates. In multi-GNSS data process-

* Corresponding author.

http://dx.doi.org/10.1016/j.asr.2014.10.002
0273-1177/

ing, however, the hardware delay is different for satellite systems even for the same type of receiver/antenna pair (Wanninger, 2012; Chen et al., 2013). Therefore, multi-GNSS data analysis requires the estimates of clock parameter together with additional inter-system bias (ISB) parameter. However, there are no conventional models for the estimation of ISB parameters within the IGS community. As a matter of result, the GLONASS satellite clocks of IGS Analysis Centers (ACs) differ in temporal reference frame or clock consistency (Schaer, 2014). The ISB results in the station clock differences when processing each system separately, and it includes the impacts of the system-dependant hardware delay terms of both station and satellite.

Therefore there should be as many clock parameters as many satellite systems that a station observes. Recent investigation shows that the difference of hardware delay between satellite systems is stable over daily interval for the same station (Dach et al., 2009, 2010; Wanninger, 2012). The clock parameter is normally treat as epoch-wise parameter, while ISB parameter is treated as daily constant (Cai and Gao, 2013; Chen et al., 2013). In case of GLONASS observations involved, there are additional inter-frequency bias (IFB) parameters caused by the frequency differences between satellites (Wanninger, 2012; Shi et al., 2013). Taking the IFBs into account, theoretically there should be as many ISB parameters as many GLONASS frequencies that a station tracks in GPS/GLONASS combined PPP. In practice, one ISB parameter is sufficient as the IFB parameter is assimilated into ambiguity parameters (Dach et al., 2010; Cai and Gao, 2013). This strategy is currently most used for the multi-GNSS PPP and has proved to be very promising (Melgard et al., 2009; Píriz et al., 2009; Dach et al., 2010; Cai and Gao, 2013).

In this paper, we analyze the correlation coefficients between ISB parameter and other parameters and apply the quantitative scaled sensitivity matrix (SSM) approach (Dong et al., 2002) for assessing the influences of unresolved ISB parameter on other parameters. Results show that there is no correlation between ISB parameter and coordinate parameters, and the ISB values can be fully assimilated into clock and ambiguity parameters. Based on this analysis, we develop a new multi-GNSS PPP model which does not include ISB parameter and observations of different GNSS systems are treated in a unified way. To verify and test the new model, we implement it to the LTW_BS software (Wang and Chen, 2011) to process 1 year GPS/GLONASS data of 53 IGS (International GNSS Service, Dow et al., 2009) stations and 1 month GPS/BDS data of 15 IGS MGEX (Multi-GNSS Experiment) stations. Two types of GPS/GLONASS and GPS/BDS combined PPP solutions are performed, one uses traditional model and the other implements the new model. Results from the two models show equivalent results, which demonstrates the efficiency and correctness of the new model. In the following, Section 2 presents the traditional multi-GNSS PPP model; Section 3 presents the new multi-GNSS PPP model; Section 4 presents data analysis and compares daily positioning qualities; finally, Section 5 summarizes the main points of this paper and discuss the perspectives of the new model.

2. Multi-GNSS PPP model based on ISB estimation

Multi-GNSS PPP refers to the combined PPP using observations from more than one satellite system, where precise satellite orbits and clocks are available. In the following formulas we use GPS/GLONASS PPP as an example, and the conclusions apply to the combined PPP for other systems as well.

2.1. GPS PPP model

The ionosphere-free (IF) pseudo-range and phase observation functions between a receiver and a GPS satellite G can be written as:

$$\begin{aligned} P^{\mathrm{G}} &= \rho^{G} + \mathrm{c}\cdot(dt_G - dt^{G}) + (b_G - b^{G}) + m^{G}\cdot ZTD^{G} + \varsigma^{G} \\ \mathrm{L}^{\mathrm{G}} &= \rho^{G} + \mathrm{c}\cdot(dt_G - dt^{G}) + (B_G - B^{G}) + N^{G} + m^{G}\cdot ZTD^{G} + \varepsilon^{G} \end{aligned} \tag{1}$$

where P^{G}, L^{G} are respectively pseudo-range and carrier phase IF observation; ρ^{G} is geometrical distance, c is light speed; dt_G is receiver clock offset, dt^{G} is satellite clock offset; b_G, b^{G} and B_G, B^{G} are the IF combined pseudo-range and carrier phase hardware delay bias for satellites ($*^{G}$) and receivers ($*_G$); N^{G} is ambiguity in meters, m^{G} and ZTD^{G} are mapping function and zenith tropospheric delay, ς^{G} and ε^{G} are noise.

The pseudo-range observation in (1) provides the reference to clock parameters. For GPS observations, the pseudo-range hardware delay biases b_G, b^{G} are assimilated into the clock offset $\mathrm{c}\cdot(dt_G - dt^{G})$ following the IGS analysis convention. The carrier phase hardware delay biases B_G, B^{G} are not considered in most GPS data processing. The carrier phase hardware bias is satellite dependent and stable over time, thus it is grouped into ambiguity (Defraigne and Bruyninx, 2007; Dach et al., 2010; Geng et al., 2010a). After applying the GPS precise satellite orbits and clocks, (1) can be rewritten as:

$$\begin{aligned} P^{\mathrm{G}} &= \rho^{G} + \mathrm{c}\cdot\bar{dt}_G + m^{G}\cdot ZTD^{G} + \varsigma^{G} \\ \mathrm{L}^{\mathrm{G}} &= \rho^{G} + \mathrm{c}\cdot\bar{dt}_G + \bar{N}^{G} + m^{G}\cdot ZTD^{G} + \varepsilon^{G} \end{aligned} \tag{2}$$

where $\bar{dt}_G$ and $\bar{N}^{G}$ are reformed station clock and ambiguity with:

$$\begin{aligned} \mathrm{c}\cdot\bar{dt}_G &= \mathrm{c}\cdot dt_G + b_G \\ \bar{N}^{G} &= N^{G} + B_G - b_G \end{aligned} \tag{3}$$

In (2), the satellite hardware delays are contained in the precise satellite clocks and are removed at the user site when applying the precise products (Defraigne and Bruyninx, 2007). Eq. (2) illustrates GPS PPP observation equation, where we see that ambiguity term is not an

integer as it contains the bias term, and the term $B_G - b_G$ refers to the un-calibrated phase delay (Ge et al., 2008). Eqs (2) and (3) apply to other GNSS systems like BDS and Galileo providing CDMA (Code Division Multiple Access) signals.

2.2. GLONASS PPP model

Extending (1) to GLONASS observations and applying the GLONASS precise satellite orbits and clocks, IF observation functions between a receiver and a GLONASS satellite R can be written as:

$$\begin{aligned} P^{\mathrm{R}} &= \rho^R + \mathrm{c}\cdot dt_R + b_R + m^R \cdot ZTD^R + \varsigma^R \\ \mathrm{L}^{\mathrm{R}} &= \rho^R + \mathrm{c}\cdot dt_R + B_R + N^R + m^R \cdot ZTD^R + \varepsilon^R \end{aligned} \tag{4}$$

Compared with (1), superscript changes from G (representing GPS) to R (representing GLONASS). The meaning of each term is similar, but now all refer to GLONASS observations.

Unlike GPS, GLONASS provides frequency division multiple access (FDMA) signal, which results in frequency differences between GLONASS satellites. Consequently, instrument hardware delays are different for a station tracking GLONASS satellites with different frequency channels (Wanninger, 2012; Chen et al., 2013; Shi et al., 2013). Hardware delay can be rewritten as a sum of a mean term and a frequency-dependent bias term as given below (Cai and Gao, 2013):

$$b_R = b_R^{avg} + \delta b_R; \quad B_R = B_R^{avg} + \delta B_R \tag{5}$$

In (5), b_R^{avg} and B_R^{avg} are the mean hardware delay for pseudo-range and phase observations. The satellite-dependent bias terms δb_R, δB_R are referred to inter-frequency bias. Substituting (5) into (4), we have the GLONASS observation equation:

$$\begin{aligned} P^{\mathrm{R}} &= \rho^R + \mathrm{c}\cdot d\bar{t}_R + \delta b_R + m^R \cdot ZTD^R + \varsigma^R \\ \mathrm{L}^{\mathrm{R}} &= \rho^R + \mathrm{c}\cdot d\bar{t}_R + \bar{N}^R + m^R \cdot ZTD^R + \varepsilon^R \end{aligned} \tag{6}$$

where $d\bar{t}_R$ and $\bar{N}^R$ are reformed station clock offset and ambiguity with:

$$\begin{aligned} \mathrm{c}\cdot d\bar{t}_R &= \mathrm{c}\cdot dt_R + b_R^{avg} \\ \bar{N}^R &= N^R + B_R^{avg} - b_R^{avg} + \delta B_R \end{aligned} \tag{7}$$

Similar to the GPS equation of (3), the mean pseudo-range hardware delay is assimilated into clock parameter and the difference between mean pseudo-range and phase hardware delay is assimilated into ambiguity parameter. The phase IFB term is treated as fractional parts of hardware delay and is assimilated into ambiguity term (Geng et al., 2010a; Dach et al., 2010; Cai and Gao, 2013). Eq. (6) contains the pseudo-range IFB term δb_R, which is satellite dependent and could not be grouped with other parameters. Theoretically, the GLONASS pseudo-range IFB could be set up as frequency-dependent unknowns in PPP processing. But this will introduce too many unknown parameters and the precision depends on the precision of pseudo-range observations. Because pseudo-range observations is normally assigned a much smaller weight compared to the carrier phase observations in GNSS data processing, δb_R can therefore be neglected and its effect will show up in the pseudo-range residuals (Geng et al., 2010a; Cai and Gao, 2013). The final GLONASS PPP observation equation can be rewritten as:

$$\begin{aligned} P^{\mathrm{R}} &= \rho^R + \mathrm{c}\cdot d\bar{t}_R + m^R \cdot ZTD^R + \varsigma^R \\ \mathrm{L}^{\mathrm{R}} &= \rho^R + \mathrm{c}\cdot d\bar{t}_R + \bar{N}^R + m^R \cdot ZTD^R + \varepsilon^R \end{aligned} \tag{8}$$

2.3. Traditional GPS/GLONASS PPP model

The traditional GPS/GLONASS PPP model requires the estimation of an additional inter-system bias parameter, the ionosphere-free (IF) pseudo-range and phase observations for the combined GPS/GLONASS PPP can be written as:

$$\begin{aligned} P^{\mathrm{G}} &= \rho^G + \mathrm{c}\cdot d\bar{t}_G + m^G \cdot ZTD + \varsigma^G \\ \mathrm{L}^{\mathrm{G}} &= \rho^G + \mathrm{c}\cdot d\bar{t}_G + \bar{N}^{\mathrm{G}} + m^G \cdot ZTD + \varepsilon^G \\ P^{\mathrm{R}} &= \rho^R + \mathrm{c}\cdot d\bar{t}_G + ISB + m^R \cdot ZTD + \varsigma^R \\ \mathrm{L}^{\mathrm{R}} &= \rho^R + \mathrm{c}\cdot d\bar{t}_G + ISB + \bar{N}^{\mathrm{R}} + m^R \cdot ZTD + \varepsilon^R \end{aligned} \tag{9}$$

In (9), the inter-system bias parameter is defined as following,

$$ISB = \mathrm{c}\cdot d\bar{t}_R - \mathrm{c}\cdot d\bar{t}_G = \mathrm{c}\cdot dt_R - \mathrm{c}\cdot dt_G + b_R^{avg} - b_G \tag{10}$$

This model has been applied in GPS/GLONASS combined PPP and is proved be more accurate and more robust than single system solution.

The modeling of ISB parameter could be in different way: as daily constant, piece wise constant (PWC) or epoch wise variable. For rigorous data analysis, epoch-wise ISB should be estimated. But this will introduce too many unknowns and reduce the efficiency of the solution. Dach et al. (2010) conducted detailed analysis on the modeling of ISB parameter by making double difference for stations equipped with different receivers. They show that the coordinate differences applying different ISB models are less than 2 mm in worst case. Considering the current PPP accuracy limits, we could conclude from their results that daily constant ISB model is sufficient for multi-GNSS PPP.

3. Simplified and unified multi-GNSS PPP model

The solution of (9) could be performed based on the least-square estimation with the complete normal equation containing all parameters generated. Based on the normal equation, we analyze the correlation coefficients between parameters. We use data of the station LPGS (La Plata, Argentina) on DOY 309, 2012. Estimated parameters include: epoch-wise station clock and static coordinates, ZTD parameter in PWC at interval of 1 h, and ISB parameter as daily constant.

We use the following function to calculate correlation coefficient between parameters:

$$r = \frac{\sigma_{AB}}{\sqrt{\sigma_A \sigma_B}} \tag{11}$$

where σ_A, σ_B, σ_{AB} are the variance and co-variance elements of parameters A and B based on the normal equation.

Fig. 1 shows the correlation coefficients between ISB parameter and coordinate parameters at first 100 epochs, where the coefficients converge to zero after the first 4 epochs.

Table 1 summarize the correlation coefficients between ISB and the other parameters of the last epoch of the daily processing. As shown in Table 1, the ISB/coordinate and ISB/ZTD correlation coefficients are near zero, which suggests that there is no correlation between ISB and these parameters. Therefore, we could remove ISB term in (9). However, the removal of ISB term introduces the change of other parameters, i.e., parameters like ambiguities and clocks will change in order to account for this new parameterization model.

To further prove the above statement and to have a quantitative gauge of the parameter assimilation, we use the SSM (Scaled Sensitivity Matrix) method (Dong et al., 2002), which is a quantitative approach for assessing the influences of unresolved parameters. Following Dong et al. (2002), we write (9) in the following form,

$$y = A_1 \cdot X_1 + A_2 \cdot X_2 \tag{12}$$

where X_2 is defined as the ISB parameter and could be removed from (12), X_1 includes the other parameters; A_1, A_2 are design matrices for corresponding parameters. The corresponding normal equation is,

$$\begin{bmatrix} N_{11} & N_{12} \\ N_{21} & N_{22} \end{bmatrix} \cdot \begin{bmatrix} X_1 \\ X_2 \end{bmatrix} = \begin{bmatrix} u_1 \\ u_2 \end{bmatrix} \tag{13}$$

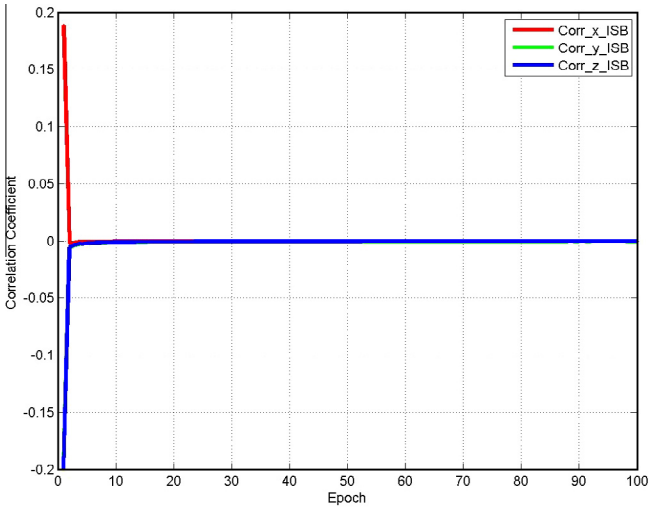

Fig. 1. Correlation coefficients between ISB parameter and coordinate parameters.

Table 1
Correlation coefficients between ISB and other parameters of GPS/GLONASS PPP.

	X	Y	Z	ZTD	$d\bar{t}_{IF,G}$	$\bar{N}^{G}_{IF}$	$\bar{N}^{R}_{IF}$
ISB	−1E−5	2E−5	1E−5	2E−5	−0.65	0.65	−0.76

According to Dong et al. (2002), since X_2 could not be resolved from the observations y, we actually solve the following normal equation

$$N_{11} X_1 = u_1 \tag{14}$$

the rigorous least squares solution of X_1 yields

$$\hat{X}_1 = N_{11}^{-1} \cdot u_1 \tag{15}$$

Replacing u_1 in (15) by (13), we obtain

$$\hat{X}_1 = X_1 + N_{11}^{-1} \cdot N_{12} \cdot X_2 \tag{16}$$

Eq. (16) indicates that the estimated values of X_1 are actually the linear combinations of X_1 and X_2 in (13). And $N_{11}^{-1} \cdot N_{12}$ are the elements of the scaled sensitivity matrix, which quantitatively defines the ratio of X_2 that assimilates to each parameter of X_1.

We calculate the scaled sensitivity matrix using the normal equation of LPGS in the above analysis and results are shown in Table 2, where the element of ISB/$\bar{N}^{G}_{IF}$ is the same for all GPS satellites and element of ISB/$\bar{N}^{R}_{IF}$ is the same for all GLONASS satellites.

According to Table 2, less than 10^{-6} parts of ISB will assimilate into coordinate parameters, which accounts to less than 1 mm for most present receivers. Less than 10^{-8} parts of ISB will assimilate into ZTD parameter, thus ZTD will not be affected by the removal of ISB.

Around 42.2% of ISB is absorbed by the clock parameter and accordingly the same amount is absorbed by GPS ambiguity parameter but with opposite sign. Thus the influence of the ISB removal for the GPS equations in (9) reflects on clock and ambiguity parameters and their influence compensates for each other.

Another 57.8% of ISB is absorbed by GLONASS ambiguity parameter. Sum the scaled sensitivity matrix element of ISB/clock and ISB/GLONASS ambiguity, we have $57.8\% + 42.2\% = 100\%$. This confirms that the sum of scaled element, which represents ratio of ISB parameter assimilated into station clock and GLONASS ambiguity parameters, equals to the original ISB in (9). Thus the influence of the ISB removal for the GLONASS equations in (9) reflects also on the clock and ambiguity parameters and the sum of their changes equal to the original ISB terms.

Based on the above discussion, the ISB in (9) could be removed and (9) could be re-written as:

$$\begin{aligned} P^{G} &= \rho^{G} + c \cdot d\bar{t}_C + m^{G} \cdot ZTD + \varsigma^{G} \\ L^{G} &= \rho^{G} + c \cdot d\bar{t}_C + \bar{N}^{G}_{C} + m^{G} \cdot ZTD + \varepsilon^{G} \\ P^{R} &= \rho^{R} + c \cdot d\bar{t}_C + m^{R} \cdot ZTD + \varsigma^{R} \\ L^{R} &= \rho^{R} + c \cdot d\bar{t}_C + \bar{N}^{R}_{C} + m^{R} \cdot ZTD + \varepsilon^{R} \end{aligned} \tag{17}$$

Table 2
Elements of the scaled sensitivity matrix between ISB and other parameters.

	X	Y	Z	ZTD	$d\bar{t}_{IF,G}$	$\bar{N}_{IF}^{G}$	$\bar{N}_{IF}^{R}$
ISB	−1E−7	6E−7	8E−7	8E−9	0.422	−0.422	0.578

where, $d\bar{t}_C$ is defined as new clock, $\bar{N}_1^G$ and $\bar{N}_1^R$ are new ambiguity terms and the other terms remain unchanged.

Eq. (17) is the simplified observation function of GPS/GLONASS PPP processing, it applies to the multi-GNSS PPP of other satellite systems. In the new model, observations of different GNSS systems is processed in an unified way as they were of the same system, and the ISB is assimilated into the clock and ambiguity parameter. Due to the much smaller weight assigned on pseudo-range observations compared to phase observations, all pseudo-range observations show big residuals and this may slow down the convergence of PPP (Geng et al., 2010b, 2011). The GPS pseudo-range residuals are close to the amount of ISB value that assimilated into the station clock parameter. The GLONASS pseudo-range residuals are close to the amount of ISB value that assimilated into the GLONASS ambiguity.

4. Data processing

To validate the new PPP model, we perform GPS/GLONASS daily static PPP for 53 IGS reference stations using data of the whole year of 2012. GPS/GLONASS kinematic PPP is performed using 1 month (January 2012) data of the 53 stations. In addition we perform GPS/BDS daily static PPP using 1 month (March, 2013) data of 15 IGS MGEX stations. Fig. 2 shows the distribution of the 68 stations.

For results evaluation and comparison, data processing is performed in the following four scenarios: GPS-only PPP, GLONASS-only PPP, traditional GPS/GLONASS and GPS/BDS combined PPP with ISB estimated as daily constant, and GPS/GLONASS and GPS/BDS combined PPP using the new model with no ISB estimated.

Moreover, precise satellite orbits and clocks from ESA, GFZ and SHA (Chen et al., 2012, 2014) are used for GPS/GLONASS PPP. Precise satellite orbits and clocks from GFZ and SHA are used for GPS/BDS PPP. We use these satellite products, rather than IGS ones, is to avoid the possible inhomogeneities of the IGS final products which can degrade the positioning quality of PPP (Teferle et al., 2007). For data modeling, we applied the absolute phase centers (Schmid et al., 2007), the phase-wind up effects (Wu et al., 1993) and the station displacement models proposed by the IERS conventions 2010 (Petit and Luzum, 2010). A cut-off angle of 7° was set for usable measurements and data sampling is set to 60 s. An elevation-dependent weighting strategy was applied to measurements at low elevations. Moreover, we estimated ZTD parameter every 1 h by applying the most recently developed GPT2 empirical slant delay model (Lagler et al., 2013). An improved version of the LTW_BS software was used (Wang and Chen, 2011).

In this following, we present how the traditional and new models agree in PPP positioning results. All the following results are based on the precise products of SHA, and PPP results based on GFZ and ESA products support the same conclusion.

4.1. Position differences between daily static PPP and IGS daily solutions

We compared our GPS/GLONASS daily position estimates with the IGS daily solutions through a 7-parameter Helmert transformation (Teferle et al., 2007; Geng et al., 2010a). We removed those position estimates with transformed residuals larger than five times the standard deviations, which amounts to less than 0.7% (118 out of 18,551

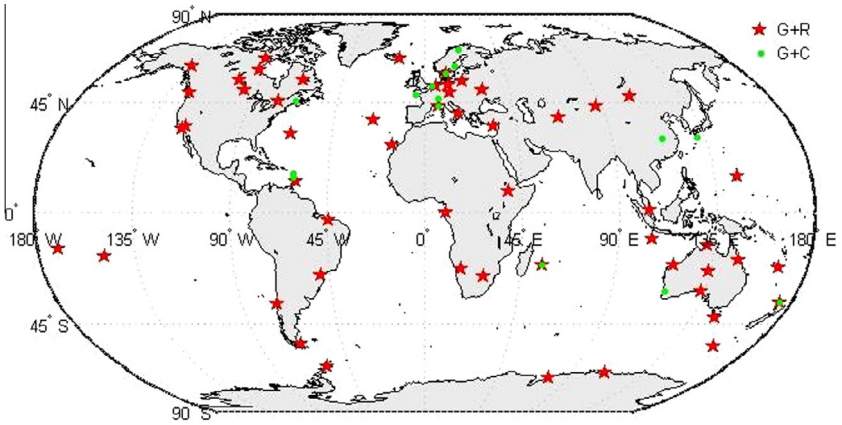

Fig. 2. The distribution of the used stations, read stars (G+R) illustrate GPS/GLONASS stations and green points (G+C) are GPS/BDS stations.

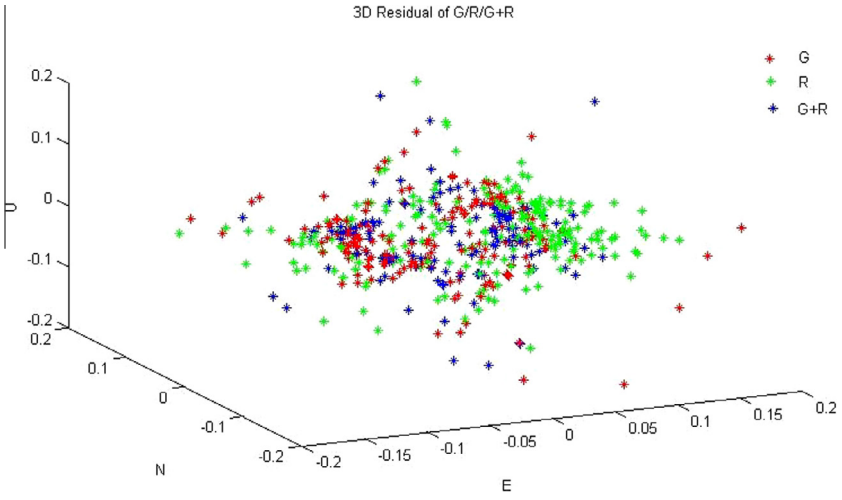

Fig. 3. Number and value of outliers in Helmert transformation between daily PPP and IGS daily solution over 1 year. PPP solutions are performed in GPS-only, GLONASS-only and GPS/GLONASS combined mode.

points). Fig. 3 shows the outliers in Helmert transformation, where the number of outliers are 168, 218 and 118 for GPS, GLONASS and GPS/GLONASS PPP, respectively. Also, the GPS/GLONASS combined PPP using new and traditional model is nearly the same and their values differ at the level of μm.

RMS statistics of the transformed residuals are used to quantitatively assess the extrinsic positioning quality. The upper plot of Fig. 4 shows for all stations the RMS statistics of coordinate differences between GPS/GLONASS PPP and IGS daily solutions. Table 3 shows the mean RMS statistics of all days for the four scenarios, where we see GPS/GLONASS combined PPP improves the RMS statistics by up to 28% compared to the single system PPP. The RMS statistics of GPS/GLONASS combined PPP using the new and traditional model are almost the same, and the bottom plot of Fig. 4 shows their RMS differences for each station. In this plot, the RMS differences are less than 1 μm in each coordinate component, verifying

Table 3
Mean RMS statistics (in mm) of residuals of the daily PPP position estimates against the IGS daily solutions in 2012.

	GPS-only	GLONASS-only	G/G trad.	G/G new
North	5.3	7.4	5.3	5.3
East	8.2	8.8	7.0	7.0
Up	15.2	18.3	13.4	13.4

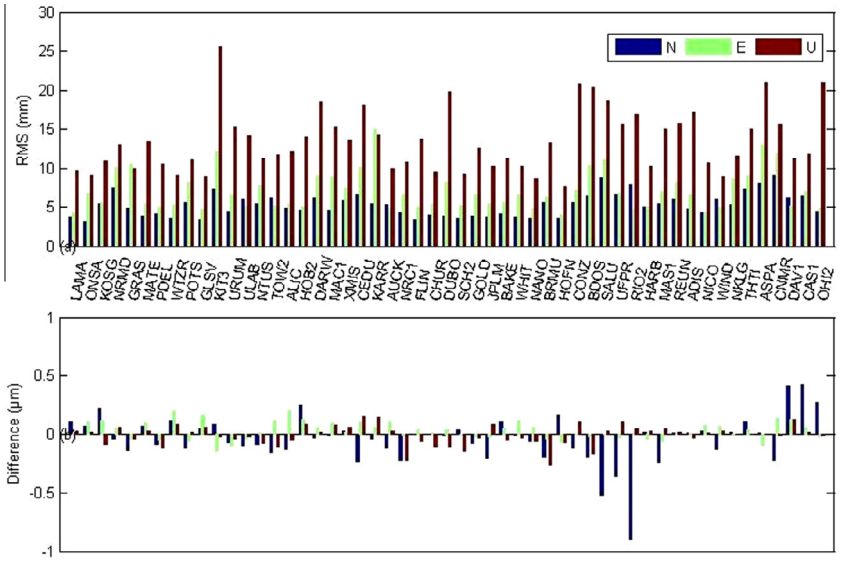

Fig. 4. (a) RMS statistics of coordinate differences between GPS/GLONASS daily static PPP and IGS daily solution for each station over one year. (b) Differences of the RMS statistics of traditional and new model for each station. A RMS is computed over the residuals of PPP position estimates against the IGS daily solutions over 1 year.

the same PPP position estimates are derived from these two models.

4.2. Position differences of daily static PPP between traditional and new model

Assessing the differences between the position estimates can directly illustrate to what extent these two models agree in their positioning results. In the following we compare the GPS/GLONASS and GPS/BDS daily static PPP results of the traditional and new models.

4.2.1. GPS/GLONASS

For each station, we computed the GPS/GLONASS PPP position differences between the two models over 1 year. All the position differences are less than 1 cm, where 13 points have difference bigger than 0.1 mm and the difference of rest 18,538 points is less than 0.1 mm. Fig. 5 shows the magnitude distribution of these coordinate differences, where the differences follow normal distributions in the North, East and Up components. The mean biases are −0.2, −0.2 and 0.3 μm and RMSs of 1.8, 3.1 and 2.6 μm for each coordinate components. These statistics are far below the formal precisions GPS solutions, implying that the position estimates of these two models are actually negligible. In addition, about 97.6% in the North, 99.2% in the East and 97.6% in the Up components of all deviations are within twice the standard deviations. Therefore, these overall good agreements verify the same position estimates of these two models.

4.2.2. GPS/BDS

For each of the 15 IGS MGEX stations, we computed the GPS/BDS daily static PPP position differences between the two models over 1 month. The biggest position difference is around 3 cm and the other points have position differences of less than 0.1 mm. Fig. 6 shows the magnitude distribution of these coordinate differences, where the differences follow normal distributions in the North, East and Up components. The mean biases are −1.1, 3.3 and 0 μm and RMSs are 2.5, 4.0 and 0.8 μm for each coordinate components. In addition, about 96.1% in the North, 93.5% in the East and 91.9% in the Up components of all deviations are within twice the standard deviations. These results again verify the same position estimates of these two models.

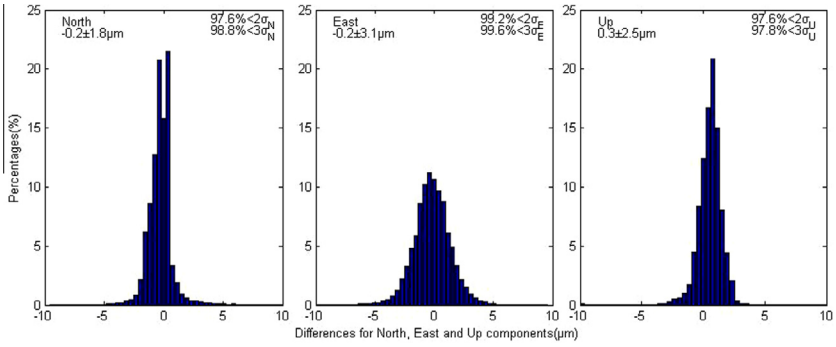

Fig. 5. Magnitude distribution of all position differences of GPS/GLONASS daily static PPP between the traditional and new models for the North, East and Up components. All subplots exhibit normal distributions. The *top-left* corner of each subplot shows the bias and the standard deviation (σ), whereas the *top-right* corner shows the percentages of deviations that are within 2σ, or larger than 3σ.

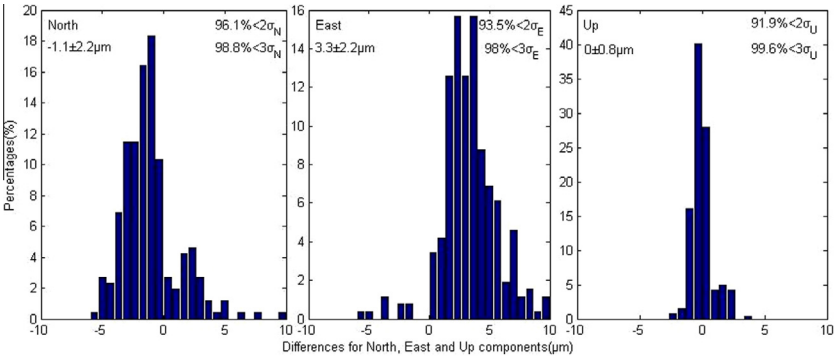

Fig. 6. Magnitude distribution of all position differences of GPS/BDS daily static PPP between the traditional and new models for the North, East and Up components. All subplots exhibit normal distributions. The *top-left* corner of each subplot shows the bias and the standard deviation (σ), whereas the *top-right* corner shows the percentages of deviations that are within 2σ, or larger than 3σ.

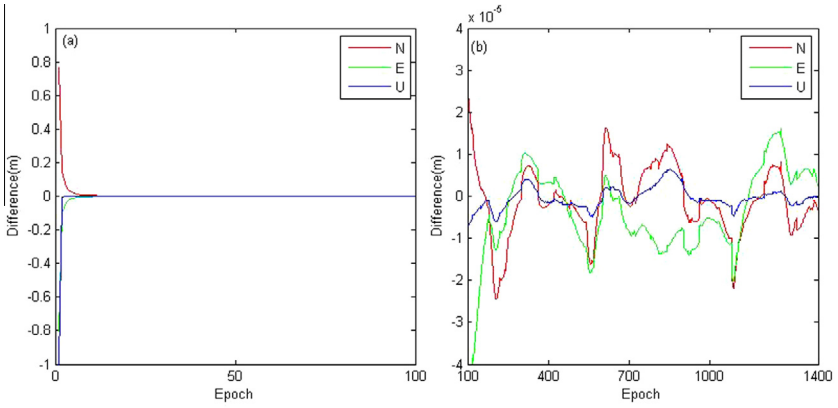

Fig. 7. Coordinate differences of kinematic PPP between the traditional and new models for ADIS, DOY 3, 2012. (a) The first 100 epochs. (b) From the 100th epoch to the end of day.

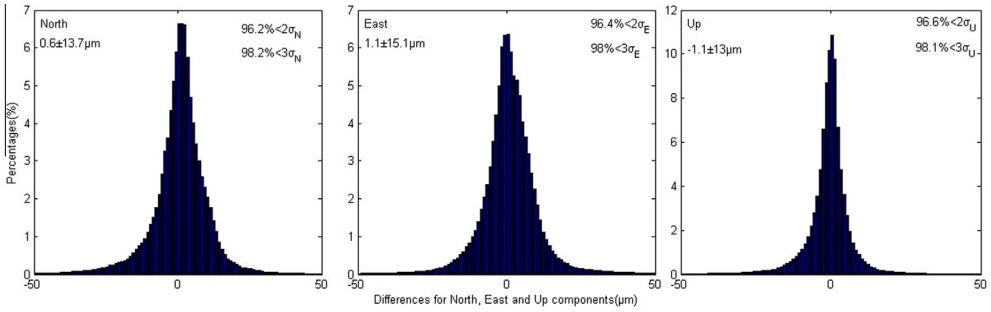

Fig. 8. Magnitude distribution of all coordinate differences of GPS/GLONASS kinematic PPP between the traditional and new models for the North, East and Up components. All subplots exhibit normal distributions. The *top-left* corner of each subplot shows the bias and the standard deviation (σ), whereas the *top-right* corner shows the percentages of deviations that are within 2σ, or larger than 3σ.

4.3. Position differences of kinematic PPP between traditional and new model

GPS/GLONASS kinematic PPP is performed using one month data of the 53 stations. Kinematic PPP results between the new and traditional models are analyzed. We first analyze the convergence of the two models. It is found that the convergences are quite close to each other. On average the position difference is less than 0.1 m after 2.4 epochs and less than 1 mm after 18.1 epochs. Fig. 7 shows the kinematic position difference of station ADIS (Addis Ababa, Ethiopia) on DOY 3, 2012. From the left plot of Fig. 7, we see that coordinate differences are less than 0.1 m after 3 epochs, while the right plot shows that the coordinate differences after the 100th epoch.

To assess the differences of the kinematic position estimates, we analyze the epoch-wise coordinates after the first 100 epochs, which are regarded as convergence period of kinematic PPP. All the position differences are less than 1 cm, where 1870 out of 1,814,500 (~0.1%) points have difference bigger than 1 mm and the difference of rest points is less than 1 mm. Fig. 8 shows the magnitude distribution of the epoch-wise coordinate differences for all stations over 1 month, where the differences follow normal distributions in the North, East and Up components. The mean biases are 0.6, 1.1 and −1.1 μm and RMSs are 13.8, 15.2 and 13.1 μm for each coordinate components. Moreover, about 96.2% in the North, 96.4% in the East and 96.6% in the Up components of all deviations in Fig. 8 are within twice the standard deviations. Thus, all these overall good agreements verify the same kinematic position estimates of these two models.

4.4. Differences of other parameters between traditional and new model

In the new multi-GNSS PPP model, the station clock and ambiguity estimates are different from that of the traditional model. These two parameters actually absorb the ISB parameters, and the percentage which goes into each parameter depends on the normal equation. Therefore, it is difficult to compare these parameters directly and have meaningful conclusion. The parameter assimilation has opposite sign for the GPS observations, thus the sum of station clock and GPS ambiguity should theoretically be the same for the traditional and new model. Therefore, we compare the sum of station clock and GPS ambiguity from the two models. The upper subplot of Fig. 9 shows the magnitude distribution of the differences for all GPS satellite/station pairs at the last epoch on all days. The mean difference is 0.1 μm and all the differences are below 3 cm with 99 out of 177,644 differences bigger than 1 mm.

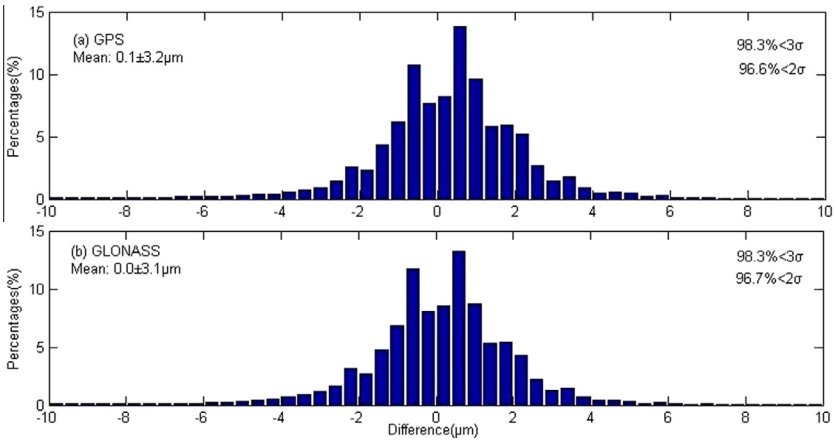

Fig. 9. Magnitude distribution of differences between the traditional and new models of (a) sum of GPS ambiguity and station clock parameters; (b) sum of GLONASS ambiguity, ISB and station clock parameters. Both plots exhibit normal distributions. The *top-left* corner of each subplot shows the bias and the standard deviation (σ), whereas the *top-right* corner shows the percentages of deviations that are within 2σ, or larger than 3σ.

For GLONASS and BDS observations, the sum of station clock and ambiguity from the new model should theoretically be the same as the sum of station clock, ISB and ambiguity of the traditional model. The bottom subplot of Fig. 9 shows the magnitude distribution of the differences for all GLONASS satellite/station pairs at the last epoch on all days. The mean difference is less than 0.1 μm and all the differences are below 1 mm with 73 out of 143,759 differences are bigger than 1 mm. Both plots show that the differences are so small, which further proves correctness of the parameter assimilation analysis and ensure the same coordinate estimates in these two models.

5. Conclusions and suggestions

In this study, we analysis the parameter correlations in multi-GNSS PPP and prove that the ISB parameter is not correlated with the coordinate and ZTD parameters. We rigorously analyze the parameter assimilation property when the ISB parameter is removed from the multi-GNSS PPP. Results show that the ISB parameter is totally assimilated into station clock and ambiguity parameters and none of ISB is absorbed by coordinate estimates. Based on these analysis, a new simplified and unified model is developed for multi-GNSS PPP.

In this new model, the ISB parameter is not explicitly defined rather it is removed in the GNSS observation equation. Applying the new model, observations of different GNSS system are treated in a unified way as they were of the same satellite system. In order to verify this new model and prove the equivalence of coordinate estimates, we compute GPS/GLONASS and GPS/BDS PPP position estimates using the traditional and new models with 1 year GPS/GLONASS data of 53 IGS stations and 1 month GPS/BDS data of 15 IGS MGEX stations.

Comparing daily static coordinate estimates between traditional and new models, mean biases of the differences are −0.2, −0.2 and 0.3 μm for GPS/GLONASS PPP, −1.1, 3.3 and 0 μm for GPS/BDS PPP, whereas the RMSs are 1.8, 3.1 and 2.6 μm for GPS/GLONASS PPP, 2.5, 4.0 and 0.8 μm for GPS/BDS PPP in the North, East and Up components respectively. Comparisons of GPS/GLONASS kinematic coordinate estimates between the two models shows mean bias of 0.6, 1.1 and -1.1 μm and RMSs of 13.8, 15.2 and 13.1 μm in the North, East and Up components respectively. The results show the coordinate differences between the two models are actually negligible, and the closeness of the coordinate estimates and RMS statistics against the IGS daily solutions overall verify the equivalence of the position estimates derived from the traditional and new models.

We have used the precise GNSS products of the GNSS analysis centers of ESA, GFZ and SHA for all the above tests. The orbit differences among these centers is at level of few cm, while their differences in satellite clocks are much bigger. This is because different strategies are applied in their ISB parameters handling and the temporal reference frames are also different. Nevertheless, the conclusion is the same. We have used GPS/GLONASS and GPS/BDS data to verify the new model, but it applies to the combined PPP for other GNSS systems.

Beside the equivalence results of the two models, there are potential advantages of the new model:

(1) Under some extreme circumstances, the traditional multi-GNSS PPP model may fail due to rank deficiency. For example, in the situation where only 4 satellites (at least one GPS and one GLONASS satellite) could be observed. Our multi-GNSS PPP approach might still obtain solutions due to omitting the ISB term (remedy the rank deficiency).

(2) The correlation between the clock and ambiguity parameters are reduced, thus stabilizing the solution using the new model.
(3) Multi-GNSS PPP realization is simplified and unified. Under this new model, observations of different GNSS system are treated in a unified way as they were of the same satellite system. Multi-GNSS PPP could be conveniently implemented in current single system PPP software module.

Implementing the new model the ambiguity and station clock absorb parts of the ISB, consequently the traditional PPP ambiguity fixing approach using un-differenced observations may not work. However, we could use the approach by making single-difference between two satellites of the same system for PPP ambiguity fixing following our new model. By making satellite-difference, the amount of ISBs assimilated into ambiguities are canceled out and the strategy of between-satellite integer ambiguity fixing could be developed.

Acknowledgments

Editor in chief Pascal Willis and three anonymous reviewers are acknowledged for their valuable suggestions. IGS community is acknowledged for providing RINEX data and orbit and clock products. This research is supported by 100 Talents Programme of the Chinese Academy of Sciences, the National Natural Science Foundation of China (NSFC) (Nos. 11273046 and 41174024), the National High Technology Research and Development Program of China (Grant Nos. 2013AA122402 and 2014AA123102) and the Shanghai Committee of Science and Technology (Grant Nos. 12DZ2273300 and 13PJ1409900).

References

Bisnath, S., Gao, Y., 2009. Current state of precise point positioning and future prospects and limitations. IAG Symp. 133, 615–623.
Cai, C., Gao, Y., 2013. Modeling and assessment of combined GPS/GLONASS precise point positioning. GPS Solut. 17 (2), 223–236.
Chen, J., Wu, B., Hu, X., et al., 2012. SHA: the GNSS analysis center at SHAO. In: Lecture Notes in Electrical Engineering, vol. 160. LNEE, pp. 213–221.
Chen, J., Pei, X., Zhang, Y., et al., 2013. GPS/GLONASS system bias estimation and application in GPS/GLONASS combined positioning. In: Lecture Notes in Electrical Engineering, vol. 244. pp. 323–333.
Chen, J., Zhang, Y., Zhou, X., et al., 2014. GNSS clock corrections densification at SHAO: from 5 minutes to 30 seconds. Sci. China Phys. Mech. Astron. 57 (1), 166–175.
Dach, R., Brockmann, E., Schaer, S., et al., 2009. GNSS processing at CODE: status report. J. Geod. 83 (3), 353–365.
Dach, R., Schaer, S., Lutz, S., et al., 2010. Combining the observations from different GNSS. In: EUREF 2010 Symposium, June 02–05, 2010, Gävle, Sweden.
Defraigne, P., Bruyninx, C., 2007. On the link between GPS pseudorange noise and day-boundary discontinuities in geodetic time transfer solutions. GPS Solut. 11 (4), 239–249.
Dong, D., Fang, P., Bock, Y., et al., 2002. Anatomy of apparent seasonal variations from GPS-derived site position time series. J. Geophys. Res. 107 (B4), 2075.
Dow, J., Neilan, R., Rizos, C., 2009. The international GNSS service in a changing landscape of global navigation satellite systems. J. Geod. 83 (3–4), 191–198.
Flohrer, C., 2008. Mutual validation of satellite-geodetic techniques and its impact on GNSS orbit modeling. In: Geodaetisch-geophysikalische Arbeiten in der Schweiz 75.
Ge, M., Gendt, G., Rothacher, M., et al., 2008. Resolution of GPS carrier-phase ambiguities in precise point positioning (PPP) with daily observations. J. Geod. 82 (7), 389–399.
Geng, J., Meng, X., Dodson, A.H., et al., 2010a. Integer ambiguity resolution in precise point positioning: method comparison. J. Geod. 84 (9), 569–581.
Geng, J., Meng, X., Dodson, A.H., et al., 2010b. Rapid re-convergences to ambiguity-fixed solutions in precise point positioning. J. Geod. 84 (12), 705–714.
Geng, J., Teferle, F.N., Meng, X., et al., 2011. Towards PPP-RTK: ambiguity resolution in real-time precise point positioning. Adv. Space Res. 47 (10), 1664–1673.
Lagler, K., Schindelegger, M., Böhm, J., et al., 2013. GPT2: empirical slant delay model for radio space geodetic techniques. Geophys. Res. Lett. 40, 1069–1073.
Melgard, T., Vigen, E., Jong, K.D., et al., 2009. G2-the first real-time GPS and GLONASS precise orbit and clock service. In: Proceedings of ION GNSS 2009, Sept 22–25. Savannah, GA, pp. 1885–1891.
Petit, G., Luzum, B. (Eds.), 2010. IERS Conventions (2010), IERS Technical Note 36. Verlagdes Bundesamts für Kartographie und Geodäsie, Frankfurt am Main, Germany.
Píriz, R., Calle, D., Mozo, A., et al., 2009. Orbits and clocks for GLONASS precise-point-positioning. In: Proceedings of ION GNSS 2009, Sept 22–25. Savannah, GA, pp. 2415–2424.
Schaer, S., 2014. Biases relevant to GPS and GLONASS data processing. In: Presentation at the IGS Workshop 2014, June 26, Pasadena, California, USA.
Schmid, R., Steigenberger, P., Gendt, G., et al., 2007. Generation of a consistent absolute phase-center correction model for GPS receiver and satellite antennas. J. Geod. 81 (12), 781–798.
Shi, C., Yi, W., Song, W., et al., 2013. GLONASS pseudorange inter-channel biases and their effects on combined GPS/GLONASS precise point positioning. GPS Solut. 17 (4), 439–451.
Teferle, F.N., Orliac, E.J., Bingley, R.M., 2007. An assessment of Bernese GPS software precise point positioning using IGS final products for global site velocities. GPS Solut. 11 (3), 205–213.
Wang, J., Chen, J., 2011. Development and application of GPS precise positioning software. J. Tongji Univ. (Natural Science) 39 (5), 764–767 (in Chinese).
Wanninger, L., 2012. Carrier-phase inter-frequency biases of GLONASS receivers. J. Geod. 86 (2), 139–148.
Wu, J.T., Wu, S.C., Hajj, G.A., et al., 1993. Effects of antenna orientation on GPS carrier phase. Manuscr. Geodaet. 18 (2), 91–98.
Zumberge, J.F., Heflin, M.B., Jefferson, D.C., et al., 1997. Precise point positioning for the efficient and robust analysis of GPS data from large networks. J. Geophys. Res. 102 (B3), 5005–5017.